Commun. Comput. Phys.
doi: 10.4208/cicp.140313.111013s

Vol. **15**, No. 4, pp. 1029-1044
April 2014

Remapping-Free Adaptive GRP Method for Multi-Fluid Flows I: One Dimensional Euler Equations

Jin Qi[1], Yue Wang[2,*] and Jiequan Li[1]

[1] *School of Mathematical Sciences, Beijing Normal University, Beijing 100875, China.*
[2] *Institute of Applied Physics and Computational Mathematics, Beijing 100094, China.*

Received 14 March 2013; Accepted (in revised version) 11 October 2013

Available online 21 January 2014

Abstract. In this paper, a remapping-free adaptive GRP method for one dimensional (1-D) compressible flows is developed. Based on the framework of finite volume method, the 1-D Euler equations are discretized on moving volumes and the resulting numerical fluxes are computed directly by the GRP method. Thus the remapping process in the earlier adaptive GRP algorithm [17,18] is omitted. By adopting a flexible moving mesh strategy, this method could be applied for multi-fluid problems. The interface of two fluids will be kept at the node of computational grids and the GRP solver is extended at the material interfaces of multi-fluid flows accordingly. Some typical numerical tests show competitive performances of the new method, especially for contact discontinuities of one fluid cases and the material interface tracking of multi-fluid cases.

AMS subject classifications: 76M12, 76N15, 76T99

Key words: The GRP method, multi-fluid flows, the Euler equations, the adaptive mesh method.

1 Introduction

Compressible multi-fluid flows can be found in a variety of scientific and engineering problems, and they are characterized by the interaction of shock waves and material interfaces. On account of those complicated fluid phenomena including strong shocks, contact discontinuities, instabilities of material interfaces, mixing processes and so on, developing numerically accurate and computationally efficient algorithms is still one of

*Corresponding author. *Email addresses:* qi_jin@iapcm.ac.cn (J. Qi), yue.wang0828@gmail.com (Y. Wang), jiequan@bnu.edu.cn (J. Li)

the challenging issues for multi-fluid simulations [1–3, 14, 20, 27, 28, 33, 34]. In this paper, we focus on the numerical methods for multi-fluid flows consisting of pure fluids separated by material interfaces.

The computation of numerical fluxes is always an important issue of numerical methods for compressible fluid dynamics. The generalized Riemann problem (GRP) method which was developed as an analytic second order accurate extension of the Godunov scheme is one of successful numerical methods to solve this problem. The basic idea of the GRP scheme consists of replacing the exact solution by a piecewise linear function and analytically solving a generalized Riemann problem at each cell interface to yield numerical fluxes, to achieve second order accuracy both in space and time. The GRP scheme was originally developed for compressible flows based on the Lagrangian formulation and the Eulerian version was always derived from the Lagrangian case [4, 7]. Then a direct Eulerian GRP scheme was presented in [8, 9, 23–25], aiming at getting rid of the auxiliary Lagrangian scheme and solving the 1-D generalized Riemann problem directly in the Eulerian frame by employing the regularity property of the Riemann invariants. Theoretically, a close coupling between the spatial and temporal evolution is recovered through the analysis of detailed wave interactions in the GRP scheme. The schemes based on the GRP method have been applied successfully to many engineering problems [5, 6, 15, 16, 23].

Computational mesh is another vital issue of numerical algorithms. In the physical and engineering problems, dynamically singular or nearly singular solutions, such as shock waves, boundary layers, etc., take place in fairly local regions. The numerical investigation of such problems may require extremely fine grids over such local domains to resolve large solution variations. Comparing with uniform grids, partly dense grids will improve the resolution of local regions and decrease the computational costs if the grids are moved at a selected adaptive speed at each time step. The adaptive mesh method [30] is one of effective moving mesh methods. A lot of important theoretical and computational progresses for partial differential equations demonstrate the advantages of the time-dependent adaptive mesh methods [10–13, 19, 21, 22, 31, 32, 36].

Based on the idea of adaptive mesh methods, the one-dimensional and two-dimensional adaptive GRP schemes by combining the Eulerian GRP scheme with the adaptive moving mesh method are developed in [17, 18]. Besides the PDE evolution, mesh redistribution is introduced in the adaptive GRP method in order to provide enough grids for specific structure of solutions such as shock waves. Thus the adaptive GRP method could improve the resolution for numerical solutions and reduce possible oscillations effectively. The computational mesh at different time steps can be generated adaptively based on a certain moving mesh method. Then physical variables and their slopes on new grids need to be updated by conservative interpolations.

On account of the complicated procedure for updating variables, this paper will develop a remapping-free adaptive GRP method. Based on the framework of finite volume method, the 1-D Euler equations are discretized on moving meshes and the resulting fluxes are computed directly by the GRP method. The material interfaces are moving

with the fluid for multi-fluid flows. Then the generalized Riemann problem for two fluids is simplified and the sonic case is avoided. Thus the GRP method can be applied for material interfaces so that the new method is available for multi-fluid problems.

The new method will bring some important benefits,

1. Since the GRP method provides detailed information of the solution to the generalized Riemann problem, it could be applied for moving meshes to derive second order numerical fluxes directly without remapping the variables and primitive slopes to the new mesh. So the interpolating procedure for conservative variables in [17] is omitted and the mesh redistribution is simplified, which also makes the whole method more efficient.
2. By adopting a flexible moving mesh strategy, the interfaces of multi-fluid flows would be kept at the nodes of spatial meshes all the time. Then the extension of the GRP solver for multi-fluid flows becomes much easier.

This paper is organized in six sections. Besides the introduction section here, the governing equations and the related discretization on moving meshes are introduced in Section 2. Then the moving mesh method is provided in Section 3, and the GRP method for the fluxes on moving meshes and the extension version for the interface fluxes of multi-fluid flows are presented in Section 4. Some numerical experiments are shown in Section 5. Finally, we present a discussion in Section 6.

2 Governing equations and the numerical algorithm

The governing equations considered here are the 1-D compressible Euler equations,

$$\mathbf{U}_t+\mathbf{F}(\mathbf{U})_x=0, \tag{2.1a}$$

$$\mathbf{U}=(\rho,\rho u,\rho E)^\top, \tag{2.1b}$$

$$\mathbf{F}(\mathbf{U})=(\rho u,\rho u^2+p,u(\rho E+p))^\top, \tag{2.1c}$$

where ρ, u, p are the density, velocity and pressure of the fluid respectively, and the total energy is $E=u^2/2+e$ with e being the specific internal energy. The above system is closed by an equation of state (EOS)

$$p=p(\rho,S). \tag{2.2}$$

The entropy S is related to other variables through the second law of thermodynamics

$$de=TdS+\frac{p}{\rho^2}d\rho. \tag{2.3}$$

Here T is the temperature. The local sound speed c is defined as

$$c^2=\frac{\partial p(\rho,S)}{\partial\rho}. \tag{2.4}$$

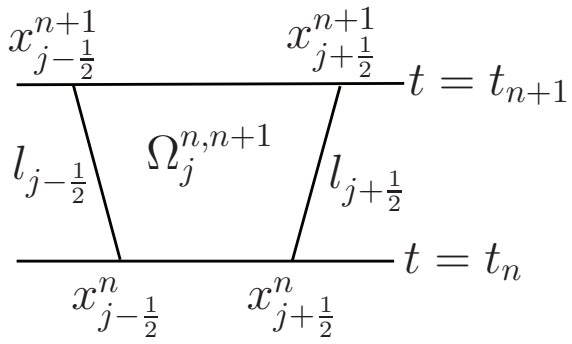

Figure 1: The control volume $\Omega_j^{n,n+1}$.

For the rest of the paper, we assume that the multi-fluid flows consist of two fluids. The EOS depends on the fluid composition, described by the variable ϕ, which governing equation has the form

$$(\rho\phi)_t+(\rho u\phi)_x=0. \tag{2.5}$$

In order to discretize the governing equations, the spacial computational domain $[a,b]$ is initially divided into M cells. We define the cells, cell centers and cell sizes at time $t=t_n=\sum_{k=1}^{n}\Delta t_k$, respectively, by

$$I_j^n=\left(x^n_{j-\frac{1}{2}},x^n_{j+\frac{1}{2}}\right),\quad x_j^n=\frac{1}{2}\left(x^n_{j-\frac{1}{2}}+x^n_{j+\frac{1}{2}}\right),\quad \Delta x_j^n=x^n_{j+\frac{1}{2}}-x^n_{j-\frac{1}{2}},\quad j=1,\cdots,M, \tag{2.6}$$

where Δt_k is the k-th time step. $\mathbf{U}_j^n$ represents the cell average of $\mathbf{U}$ over cell I_j^n. At each time step, the spatial mesh is redistributed by

$$x^{n+1}_{j-\frac{1}{2}}=x^n_{j-\frac{1}{2}}+D^n_{j-\frac{1}{2}}(t_{n+1}-t_n), \tag{2.7}$$

where $D^n_{j-1/2}$ is mesh moving velocity decided by a moving mesh method. When $D_j^n\equiv 0$, the computational mesh becomes Eulerian grids. When $D_j^n\equiv u_j^n$, the computational mesh becomes Lagrangian grids.

The control volume $\Omega_j^{n,n+1}$ (see Fig. 1) considered here is not a rectangle and its boundary $\partial\Omega_j^{n,n+1}$ is composed of the following four lines:

(a) $l_{j-\frac{1}{2}}$: $x=x^n_{j-\frac{1}{2}}+D^n_{j-\frac{1}{2}}(t-t_n)$, for $t\in[t_n,t_{n+1})$.

(b) $l_{j+\frac{1}{2}}$: $x=x^n_{j+\frac{1}{2}}+D^n_{j+\frac{1}{2}}(t-t_n)$, for $t\in[t_n,t_{n+1})$.

(c) $t=t_n$, $x\in\left[x^n_{j-\frac{1}{2}},x^n_{j+\frac{1}{2}}\right]$.

(d) $t=t_{n+1}$, $x\in\left[x^{n+1}_{j-\frac{1}{2}},x^{n+1}_{j+\frac{1}{2}}\right]$.

Then the Euler equations (2.1a) can be discretized by integrating the equations over $\Omega_j^{n,n+1}$ as

$$\int_{\partial\Omega_j^{n,n+1}}(\mathbf{F},\mathbf{U})\cdot\mathbf{n}d\mathbf{s}=0, \tag{2.8}$$

where $\mathbf{n}$ is the outward normal vector of $\partial\Omega_j^{n,n+1}$ and $d\mathbf{s}$ is a directional infinitesimal element. Eq. (2.8) is often referred to as the arbitrary Lagrangian-Eulerian (ALE) form of the conservation laws on the moving meshes. The discrete formulation of (2.8) is

$$\Delta x_j^{n+1}\mathbf{U}_j^{n+1}-\Delta x_j^n\mathbf{U}_j^n+\Delta t_n(\hat{\mathbf{F}}_{j+\frac{1}{2}}-\hat{\mathbf{F}}_{j-\frac{1}{2}})=0, \tag{2.9}$$

where

$$\mathbf{U}_j^{n+1}=\frac{1}{\Delta x_j^{n+1}}\int_{I_j^{n+1}}\mathbf{U}(x,t_{n+1})dx,$$
$$\hat{\mathbf{F}}_{j+\frac{1}{2}}=\frac{1}{\Delta t_n\sqrt{1+(D_{j+\frac{1}{2}}^n)^2}}\int_{l_{j+\frac{1}{2}}}\hat{\mathbf{F}}(x,t)ds,$$

and

$$\hat{\mathbf{F}}=\big(\rho(u-D_{j+\frac{1}{2}}^n),\rho u(u-D_{j+\frac{1}{2}}^n)+p,\rho E(u-D_{j+\frac{1}{2}}^n)+up\big)^\top.$$

Based on the above formulations, the computation of compressible multi-fluid problems is considered. By tracking the material interface as a Lagrangian point, the Eq. (2.5) is satisfied naturally. So the computation of fluxes for multi-fluid flows is simplified into solving single fluid generalized Riemann problems and one generalized Riemann problem with two fluids separated by the material interface. The GRP solver is developed accordingly to solve the resulting generalized Riemann problems with relevant EOS on moving grids. Our algorithm is described briefly as follows:

Algorithm 2.1.

1. Given the initial mesh $\{x_{j-1/2}^n\}$ and the piecewise initial data at time $t=t_n$,

   $$\mathbf{U}_j(x,t_n)=\mathbf{U}_j^n+(\mathbf{U}_x)_j^n(x-x_j^n),\quad x\in(x_{j-\frac{1}{2}}^n,x_{j+\frac{1}{2}}^n),$$

   determine the moving velocity $\{D_{j+1/2}^n\}$ of the initial mesh and then derive the new adaptive mesh $\{x_{j-1/2}^{n+1}\}$ at $t=t_{n+1}$.
2. Evaluate the numerical fluxes $\{\hat{\mathbf{F}}_{j+1/2}\}$ by remapping-free adaptive GRP solver.
3. Compute $\mathbf{U}_j^{n+1}$ by (2.9) and derive the derivatives $\{(\mathbf{U}_x)_j^{n+1}\}$ by $\{\mathbf{U}_j^{n+1}\}$.
4. Back to Step 1 until time is up.

In the next sections, we will focus on the details of mesh redistribution and flux computation.

3 Mesh generation

In our mesh redistribution method, computational mesh is divided into different parts to represent different fluids respectively. Material interfaces are treated as Lagrangian moving points to avoid mixing cells firstly. Then the mesh for each fluid region is redistributed separately by adaptive mesh methods. The algorithm comprises of the following two steps.

Step 1. Track material interfaces.

In order to move a material interface in the Lagrangian mode, the key ingredient is to compute the moving speed of the material interface. Because the material interface is always fixed at the mesh boundary, the problem is changed into computing the nodal fluid velocity. Here the nodal moving speeds $\{D^n_{j+1/2}|_{interfaces}\}$ are derived by

$$D^n_{j+\frac{1}{2}}=u^*+\frac{1}{2}\Delta t\sqrt{1+(u^*)^2}\Big(\frac{\partial u}{\partial \mathbf{n}}\Big)^n_{l^*_{j+\frac{1}{2}}}, \tag{3.1}$$

where u^* is approximated by the solution of the associated Riemann problem (4.5) in the star region described in the next section and $(\partial u/\partial \mathbf{n})^n_{l^*_{j+1/2}}$ is derived by the GRP method with

$$l^*_{j+\frac{1}{2}}: x=x^n_{j+\frac{1}{2}}+u^*(t-t_n) \quad \text{and} \quad \mathbf{n}=\frac{1}{\sqrt{1+(u^*)^2}}(u^*,1).$$

Then we get $\{x^{n+1}_{j+1/2}|_{interfaces}\}$ by (2.7), which is second order accurate.

Step 2. Redistribute meshes in each fluid region.

Winslow's variable diffusion method [37] based on the following 1-D Euler-Lagrange equation is adopted to implement the redistribution,

$$(\omega x_\xi)_\xi=0, \tag{3.2}$$

where ξ denotes the reference coordinate. ω is the monitor function to control the mesh moving. An appropriate choice of the monitor will produce grids with our desired qualities such as smoothness, reflecting fluid properties and so on. Since the choice of the monitor function is not the main task in this paper, so we will just use an effective one [30],

$$\omega=\sqrt{1+\alpha_1\Big(\frac{u_\xi}{\max|u_\xi|}\Big)^2+\alpha_2\Big(\frac{S_\xi}{\max|S_\xi|}\Big)^2}, \tag{3.3}$$

where S is entropy and the parameters α_i $(i=1,2)$ are nonnegative constants.

In practice, we usually use Gauss-Seidel iteration to solve Eq. (3.2) and yield the desired mesh $\{x^{n+1}_{j+1/2}|_{non-interfaces}\}$.This method is easily coded and effective in many applications [30].

In the above procedures, the only task is to rezone the mesh at current time step. The conservative properties of physical variables are preserved by the ALE formulations without conservative interpolations between the two sets of meshes that were done in the earlier adaptive GRP [17,18]. So the earlier mesh redistribution step is simplified and more flexible and effective mesh generation methods could be used.

4 Numerical fluxes for multi-fluid flows: based on the GRP solver

The evolution of physical variables depends on the flux evaluation on a reference of the moving frame with grid velocities chosen by the last section. In this paper, we shall use the GRP method for the flux evaluation. The main reason is that GRP solver is second-order accurate in any time-space directions. Moreover, the GRP method could be extended for the material interfaces of multi-fluid flows.

In order to obtain the numerical flux $\hat{\mathbf{F}}_{j+1/2}$ with the temporal accuracy of second order, the middle point value is used to approximate the flux

$$\int_{l_{j+\frac{1}{2}}} (\mathbf{F}(\mathbf{U}(x,t)),\mathbf{U}(x,t))\cdot\mathbf{n}_\perp d\mathbf{s} = \int_{l_{j+\frac{1}{2}}} \frac{\mathbf{F}(\mathbf{U}(x,t)) - D^n_{j+\frac{1}{2}}\mathbf{U}(x,t)}{\sqrt{1+(D^n_{j+\frac{1}{2}})^2}} ds, \tag{4.1}$$

where

$$l_{j+\frac{1}{2}} : x = x_{j+\frac{1}{2}}(t) = x^n_{j+\frac{1}{2}} + D^n_{j+\frac{1}{2}}(t-t_n), \quad t\in[t_n,t_{n+1}),$$

and

$$\mathbf{n}_\perp = \frac{1}{\sqrt{1+(D^n_{j+\frac{1}{2}})^2}}(1,-D^n_{j+\frac{1}{2}})^\top$$

is the outer normal vector of $\Omega^{n,n+1}_j$ along $l_{j+1/2}$. Thus the numerical flux $\hat{\mathbf{F}}_{j+1/2}$ is derived by

$$\hat{\mathbf{F}}_{j+\frac{1}{2}} = \mathbf{F}\Big(\mathbf{U}^{n+\frac{1}{2}}_{l_{j+\frac{1}{2}}}\Big) - D^n_{j+\frac{1}{2}}\mathbf{U}^{n+\frac{1}{2}}_{l_{j+\frac{1}{2}}}, \tag{4.2a}$$

$$\mathbf{U}^{n+\frac{1}{2}}_{l_{j+\frac{1}{2}}} = \mathbf{U}^n_{l_{j+\frac{1}{2}}} + \frac{1}{2}\Delta t\sqrt{1+(D^n_{j+\frac{1}{2}})^2}\Big(\frac{\partial\mathbf{U}}{\partial\mathbf{n}}\Big)^n_{l_{j+\frac{1}{2}}} = \mathbf{U}^n_{l_{j+\frac{1}{2}}} + \frac{1}{2}\Delta t\Big[(\mathbf{U}_t)^n_{l_{j+\frac{1}{2}}} + D^n_{j+\frac{1}{2}}(\mathbf{U}_x)^n_{l_{j+\frac{1}{2}}}\Big], \tag{4.2b}$$

where

$$\mathbf{n} = \frac{1}{\sqrt{1+(D^n_{j+\frac{1}{2}})^2}}(D^n_{j+\frac{1}{2}},1)^\top,$$

and $\mathbf{U}^n_{l_{j+1/2}}$, $(\mathbf{U}_t)^n_{l_{j+1/2}}$, $(\mathbf{U}_x)^n_{l_{j+1/2}}$ and $(\partial\mathbf{U}/\partial\mathbf{n})^n_{l_{j+1/2}}$ are the instantaneous value of $\mathbf{U}$ and its time, spatial and directional derivatives when t is close to t_{n+} along $l_{j+1/2}$ which are

solved by the generalized Riemann problem

$$\mathbf{U}(x,t_n)=\begin{cases}\mathbf{U}_j^n+(\mathbf{U}_x)_j^n(x-x_j^n), & x\in\left(x_{j-\frac{1}{2}}^n,x_{j+\frac{1}{2}}^n\right),\\ \mathbf{U}_{j+1}^n+(\mathbf{U}_x)_{j+1}^n(x-x_{j+1}^n), & x\in\left(x_{j+\frac{1}{2}}^n,x_{j+\frac{3}{2}}^n\right).\end{cases}\tag{4.3}$$

Now the main issue here is how to calculate this generalized Riemann problem using as much information of the Euler equations (2.1a)-(2.1c) as possible.

In order to simplify notations, the point $(x,t)=(x_{j+1/2},t_n)$ in the above generalized Riemann problem is moved to $(x,t)=(0,0)$. Then we only need to discuss next two cases of generalized Riemann problems. They have the same initial conditions for $\mathbf{U}$,

$$\mathbf{U}(x,0)=\begin{cases}\mathbf{U}_l+x\mathbf{U}_l', & x\le 0,\\ \mathbf{U}_r+x\mathbf{U}_r', & x>0,\end{cases}\tag{4.4}$$

but with different EOS separately

(1) (One-fluid) $p=p(\rho,S)$ for all x.

(2) (Two-fluid) $p=p_1(\rho,S)$ for $x\le 0$ and $p=p_2(\rho,S)$ for $x>0$.

Denote

$$\mathbf{n}=\frac{1}{\sqrt{1+D^2}}(D,1)\quad\text{and}\quad\frac{D\mathbf{U}}{D\mathbf{n}}=\mathbf{U}_t+D\mathbf{U}_x.$$

By recalling (4.2b), we only need to derive the instantaneous values $\mathbf{U}_*$ and $(D\mathbf{U}/D\mathbf{n})_*$ instead of the directional derivative $(\partial\mathbf{U}/\partial\mathbf{n})_*$ when t is close to 0_+ along $\hat{l}:x=Dt$.

4.1 The Riemann problem for multi-fluid flows

First of all, we need to solve the associated Riemann problem

$$\mathbf{U}(x,0)=\begin{cases}\mathbf{U}_l, & x\le 0,\\ \mathbf{U}_r, & x>0,\end{cases}\tag{4.5}$$

for (2.1a)-(2.1c) with proper EOS to obtain the self-similar solution $\mathbf{U}(x,t)=\mathbf{U}(x/t)=R^A(x/t;\mathbf{U}_l,\mathbf{U}_r)$. Then we could derive the instantaneous value of $\mathbf{U}$

$$\mathbf{U}_*=R^A(D;\mathbf{U}_l,\mathbf{U}_r).$$

The basic configurations of the Riemann problem include two rarefaction waves, two shocks and shock-rarefaction waves besides the contact discontinuity (Fig. 2(b)). For each configuration we can obtain a nonlinear system for the constant velocity u^* and pressure p^* in the star region,

$$\begin{cases}u^*-u_l+(p^*-p_l)/g_l=0,\\ u^*-u_r-(p^*-p_r)/g_r=0,\end{cases}\tag{4.6}$$

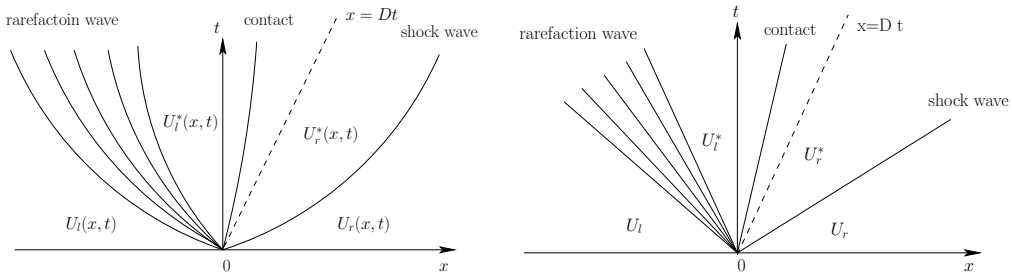

Figure 2: Typical wave configurations of the generalized Riemann problem (a) and the associated Riemann problem (b).

where g_i, $i=l,r$, are

$$g_i=\begin{cases}\sqrt{\rho^*\rho_i(p^*-p_i)/(\rho^*-\rho_i)}, & p>p_i,\\ (p^*-p_i)\Big(\displaystyle\int_{p_i}^{p^*}1/(\rho c)dp\Big)^{-1}, & p<p_i.\end{cases}\tag{4.7}$$

Then the pressure p^* in the star region is derived by solving a single algebraic equation

$$F(p^*):=f_l(p^*)+f_r(p^*)-u_l+u_r=0,\tag{4.8}$$

where $f_i=(p^*-p_i)/g_i$. Since for the polytropic gases, the pressure function $F(p)$ has particularly simple behavior (concave) and the analytical expressions for the derivatives of $F(p)$ are available, we use a Newton-Raphson [26] iteration to find the root of $F(p)=0$ [35]. For more general cases, the algebraic equation $F(p)=0$ may not have the same simple behavior. Some techniques could be applied for solving this equation more conveniently [28]. Furthermore, the velocity u^* and density ρ_l^* and ρ_r^* in the star region are obtained based on (4.6) and the EOS. Then the instantaneous value $\mathbf{U}_*$ is derived by the location of $\hat{l}:x=Dt$ in the whole wave configuration.

It should be noticed that the choice of precise EOS for (4.7) is very important. For the one-fluid case, only one EOS $p=p(\rho,S)$ is applied to (4.7). For the multi-fluid case, we know that the contact discontinuity is just the interface between two fluids based on moving mesh strategy in Section 3. Thus in (4.7), g_l will be computed by using the EOS $p=p_1(\rho,S)$ and the formulation of g_r will use the EOS $p=p_2(\rho,S)$. Moreover, since the contact discontinuity of this Riemann solution coincides with $\hat{l}:x=Dt$, the instantaneous values u_* and p_* are picked by u^* and p^* respectively, and ρ_* is computed by the detailed wave configuration. Thus the instantaneous value $\mathbf{U}_*$ is derived on the material interface.

4.2 The GPR method for multi-fluid flows

With the above Riemann solution, it is clear that only $(D\mathbf{U}/D\mathbf{n})_*$ (or $(\mathbf{U}_t)_*$ and $(\mathbf{U}_x)_*$) is left to be defined for the second order numerical fluxes. The GRP method we used here

is from [9] where a direct and simple derivation of the Eulerian generalized Riemann problem for compressible fluid flows is provided on fixed meshes. In this section, we will extend it onto one dimensional moving meshes and then apply it for multi-fluid flows at the material interfaces.

In the GRP approach, if $\hat{l}$:$x=Dt$ locates in the star region (Fig. 2(a)), since the flow variables u and p are regular across the contact discontinuity in the star region, we can first calculate $(Du/D\mathbf{n})_*$ and $(Dp/D\mathbf{n})_*$, and then derive $(D\rho/D\mathbf{n})_*$. The main feature of the GRP scheme is the resolution of centered rarefaction waves. For the associated Riemann problem, the Riemann variants are constant throughout an isentropic rarefaction waves. That means they are still regular inside the nonisentropic rarefaction waves in the generalized Riemann problems. Thus the Riemann variants and characteristic coordinates are used to resolve the rarefaction waves at the singularity points. Then a linear relation between $(Du/D\mathbf{n})_*$ and $(Dp/D\mathbf{n})_*$ is derived. In addition, in the sonic case, one of the characteristic curves inside the rarefaction wave is tangential to $\hat{l}: x=Dt$. Then there is enough information available from the rarefaction wave to calculate the time derivatives of all flow variables. For shock waves, the Rankine-Hugoniot relations are used to obtain another linear relation between $(Du/D\mathbf{n})_*$ and $(Dp/D\mathbf{n})_*$. Finally, $(Du/D\mathbf{n})_*$ and $(Dp/D\mathbf{n})_*$ are solved by a linear algebraic systems containing two equations.

Similar to the last section, we can derive $(Du/D\mathbf{n})_*$ and $(Dp/D\mathbf{n})_*$ for one dimensional moving meshes, and the interface fluxes for multi-fluids are summarized together in the following proposition for non-sonic cases.

Proposition 4.1. (see [9]). Let $\mathbf{U}_*$ and $(D\mathbf{U}/D\mathbf{n})_*$ be the instantaneous values of $\mathbf{U}$ and $D\mathbf{U}/D\mathbf{n}$ as t is close to 0_+ along $\hat{l}$:$x=Dt$. Then $(Du/D\mathbf{n})_*$ and $(Dp/D\mathbf{n})_*$ are determined by solving a pair of linear equations,

$$a_l\Big(\frac{Du}{D\mathbf{n}}\Big)_*+b_l\Big(\frac{Dp}{D\mathbf{n}}\Big)_*=d_l, \tag{4.9a}$$

$$a_r\Big(\frac{Du}{D\mathbf{n}}\Big)_*+b_r\Big(\frac{Dp}{D\mathbf{n}}\Big)_*=d_r, \tag{4.9b}$$

where the coefficients a_l, b_l and d_l depend on $\mathbf{U}_*$, $\mathbf{U}_l$, $\mathbf{U}_l'$ and D; and a_r, b_r and d_r depend on $\mathbf{U}_*$, $\mathbf{U}_r$, $\mathbf{U}_r'$ and D. All coefficients which are related to the EOS can be found in [9]. Particularly for the multi-fluid cases, the coefficients a_l, b_l and d_l are related with $p=p_1(\rho,S)$ and a_r, b_r and d_r are related with $p=p_2(\rho,S)$. Then $(D\rho/D\mathbf{n})_*$ is given by the EOS $p=p(\rho,S)$,

$$dp=c^2d\rho+\frac{\partial p}{\partial S}dS. \tag{4.10}$$

Remark 4.1. 1. If $D<u_l-c_l$ (the case $D>u_r+c_r$ is dealt similarly), then $\hat{l}$:$x=Dt$ locates in the left region in which $\mathbf{U}$ is continuous. Then the time and spatial derivatives of $\mathbf{U}$ along $\hat{l}: x=Dt$ as $t\to 0$ are

$$(\mathbf{U}_x)_*=\mathbf{U}_l', \quad (\mathbf{U}_t)_*=-\frac{\partial \mathbf{F}}{\partial \mathbf{U}}(\mathbf{U}_l)\mathbf{U}_l'.$$

Thus $(D\mathbf{U}/D\mathbf{n})_*$ equals to

$$\left(\frac{D\mathbf{U}}{D\mathbf{n}}\right)_* = (\mathbf{U}_t)_* + D(\mathbf{U}_x)_*.$$

2. For the multi-fluids case, the interface is just the contact discontinuity of the related generalized Riemann problem. So $(Du/Dt)_*$ and $(Dp/Dt)_*$ are obtained from (4.9a)-(4.9b) with different EOS. Here $Du/Dt = u_t + uu_x$ and $Dp/Dt = p_t + up_x$.

The proof of this proposition and the details of the coefficients can be found in [9]. Next we will provide a proposition for the sonic case which is slightly different with [9] when any direction $D/D\mathbf{n}$ is used. It should be noticed that the sonic case will only occur in one fluid based on Remark 4.1.

Proposition 4.2. (sonic case). If $\hat{l}: x = Dt$ is located inside the rarefaction wave associated with the $u-c$ characteristic family. Then we have

$$\left(\frac{Du}{D\mathbf{n}}\right)_* = d_l(D), \quad \left(\frac{Dp}{D\mathbf{n}}\right)_* = \rho_*(u_* - D)d_l(D), \tag{4.11}$$

where $d_l = d_l(\beta)$ is defined in [9], $\beta \in (u_l - c_l, u^* - c_l^*)$.

5 Numerical results

In this section, we will provide some numerical examples to validate the new scheme. In all cases, the time step is determined by

$$\Delta t = \nu * \min_j \Delta x_j / \max_j (|u_j| + c_j), \tag{5.1}$$

where ν is the CFL number picked as 0.5 and Δx_j is the length of cell $I_j = [x_{j-1/2}, x_{j+1/2}]$. Here and after, we suppress the superscript n for simplicity. The EOS for all numerical cases are the one for polytropic gases

$$p = (\gamma - 1)\rho e. \tag{5.2}$$

In this paper, the reconstruction is applied to the primitive flow variables and the limiter used is the minmod limiter

$$(\mathbf{U}_x)_j = minmod\left\{\theta \cdot \frac{2(\mathbf{U}_{j+1} - \mathbf{U}_j)}{\Delta x_j + \Delta x_{j+1}}, \frac{\mathbf{U}_{j+\frac{1}{2}} - \mathbf{U}_{j+\frac{1}{2}}}{\Delta x_j}, \theta \cdot \frac{2(\mathbf{U}_j - \mathbf{U}_{j-1})}{\Delta x_j + \Delta x_{j-1}}\right\}, \tag{5.3}$$

where $\mathbf{U}_{j+1/2}$ is computed by the GRP solver and $\theta \in [1,2)$. Here θ is chosen by 1.9. After reconstruction, the flow variable $\mathbf{U}$ is distributed linearly in cell I_j,

$$\mathbf{U}_j(x) = \mathbf{U}_j + (\mathbf{U}_x)_j(x - x_j).$$

In this section, the remapping-free adaptive GRP method is denoted by the RA-GRP method for short and RA-Godunov method denotes the corresponding first order scheme.

Example 5.1. (The contact discontinuity problem). This test is a Riemann problem with initial data

$$\rho=1.0, \quad u=1.0, \quad p=1.0, \quad \gamma=1.4, \quad 0<x<0.5, \tag{5.4a}$$
$$\rho=0.125, \quad u=1.0, \quad p=1.0, \quad \gamma=1.4, \quad 0.5<x<1, \tag{5.4b}$$

which only contains one contact discontinuity. The RA-GRP method is compared with the GRP method and the exact solution in Fig. 3 at $t=0.15$. The result shows that the RA-GRP can capture the contact discontinuity exactly without any dissipation.

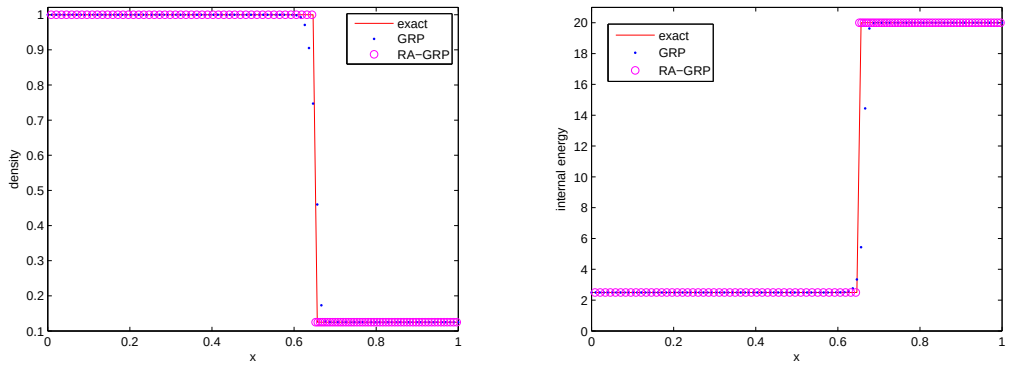

(a) (b)

Figure 3: The contact discontinuity problem with 100 cells.

Example 5.2. (The Sod problem). This test is the Sod problem. The initial conditions in the present computation are the following:

$$\rho=1.0, \quad u=0.0, \quad p=1.0, \quad \gamma=1.4, \quad 0<x<0.5, \tag{5.5a}$$
$$\rho=0.125, \quad u=0.0, \quad p=0.1, \quad \gamma=1.4, \quad 0.5<x<1. \tag{5.5b}$$

Fig. 4 shows the results computed by the RA-GRP method, the GRP method and the exact solution at $t=0.15$. 60 cells are used here. We could observe that RA-GRP method can provide competitive numerical results compared with the adaptive GRP method [17] (see Fig. 5.1 in page 1456), and especially capture the contact discontinuity with less cells.

Example 5.3. (The Woodward and Colella problem). This test is the Woodward and Colella problem. The initial conditions in the present computation are the following:

$$\rho=1.0, \quad u=0.0, \quad p=1000.0, \quad \gamma=1.4, \quad 0<x<0.1, \tag{5.6a}$$
$$\rho=1.0, \quad u=0.0, \quad p=0.01, \quad \gamma=1.4, \quad 0.1<x<0.9, \tag{5.6b}$$
$$\rho=1.0, \quad u=0.0, \quad p=100.0, \quad \gamma=1.4, \quad 0.9<x<1. \tag{5.6c}$$

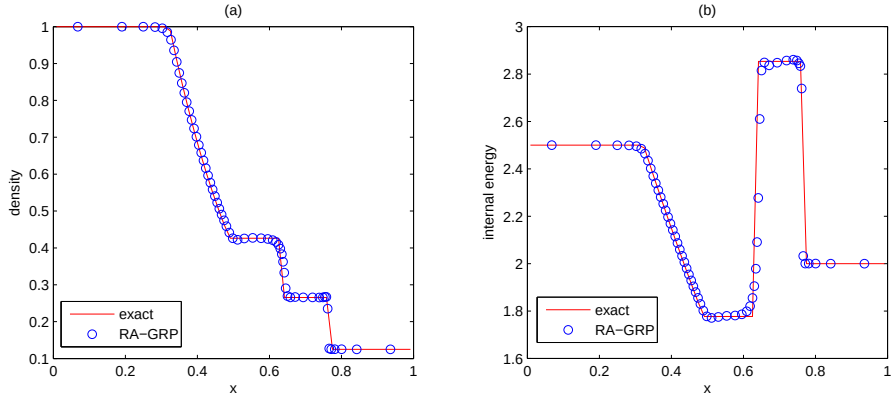

Figure 4: The Sod problem with 60 cells.

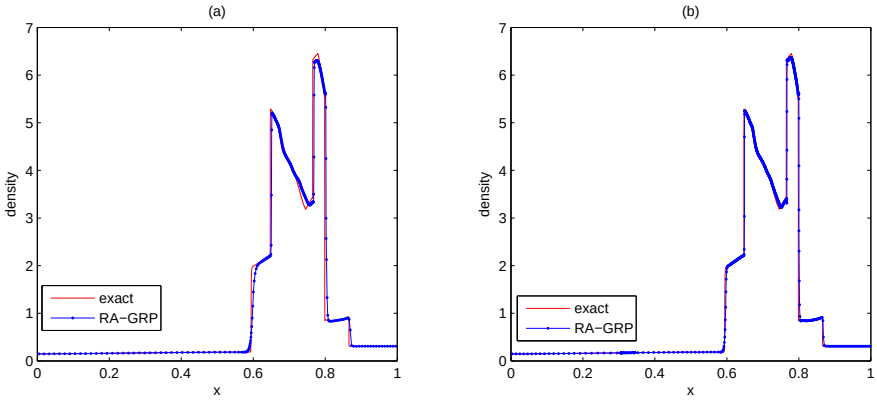

Figure 5: The Woodward and Colella problem with 400 cells (a) and 800 cells (b). The exact solution is approximated by the same scheme with 4000 cells.

Fig. 5 shows the results computed by the RA-GRP method and the exact solution at $t=0.038$ by 400 cells (Fig. 5(a)) and 800 cells (Fig. 5(b)). We could observe that RA-GRP method can provide competitive numerical results compared with the remapping-free ALE-type kinetic method in [29] (see Fig. 4 in page 3163) and especially capture the contact discontinuity more sharply.

Example 5.4. (The material interface problem). This case is the material interface problem, whose solution represents a single contact discontinuity in gas dynamics. The initial conditions in the present computation are the following:

$$\rho=1.0, \quad u=1.0, \quad p=1.0, \quad \gamma=1.4, \quad 0<x<0.5, \tag{5.7a}$$

$$\rho=0.125, \quad u=1.0, \quad p=1.0, \quad \gamma=1.2, \quad 0.5<x<1. \tag{5.7b}$$

Fig. 6(a) shows that both the RA-Godunov method and the RA-GRP method can capture the material interface precisely at time $t=0.2$.

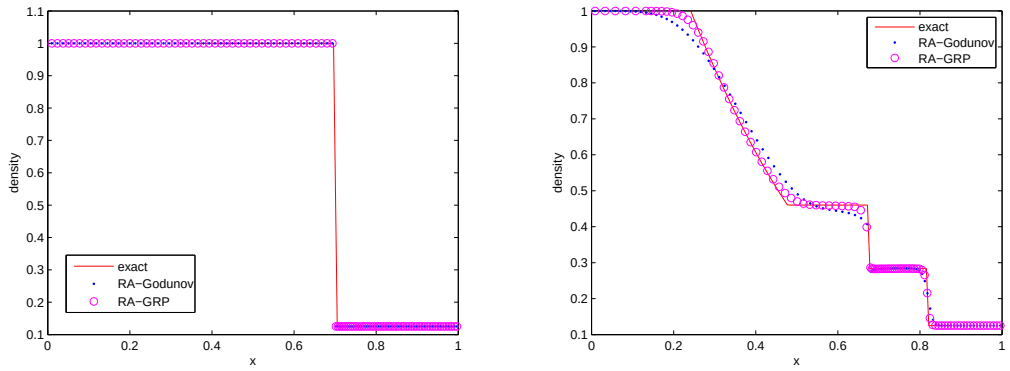

(a) (b)

Figure 6: (a) The material interface problem with 100 cells; (b) The shocktube problem with different adiabatic indexes with 100 cells.

Example 5.5. (The shocktube problem with different adiabatic indexes). The Sod shocktube problem, now with two different polytropic gases, is considered here. The initial conditions in the present computation are the following:

$$\rho=1.0, \quad u=0.0, \quad p=1.0, \quad \gamma=1.667, \quad 0<x<0.5, \tag{5.8a}$$

$$\rho=0.125, \quad u=0.0, \quad p=0.1, \quad \gamma=1.2, \quad 0.5<x<1. \tag{5.8b}$$

Fig. 6(b) compares the RA-Godunov method and the RA-GRP method with the exact solution at $t=0.2$. From the numerical results around the rarefaction wave, contact discontinuity and shock, we can observe that RA-GRP method improves the resolution of the whole wave configuration.

6 Conclusions

In this paper, a remapping-free GRP method is developed for both one-fluid and multi-fluid problems. Based on the ALE conservative discretization, the revolution between two different sets of computational meshes could be implemented directly by extended GRP solver without conservative remapping. Moreover, by synchronizing the movement of computational mesh with that of the multi-flows at material interfaces, the interface of two fluids will be kept at the node of computational grids. So the GRP solver is also developed to the resulting multi-fluid general Riemann problems accordingly. Numerical results show the new method's accuracy and efficiency for solving problems with shocks and contact discontinuities.

This is the first paper of our serial work. The two dimensional remapping-free GRP method is under investigation. Two-dimensional adaptive mesh moving method and two-dimensional GRP solver for multi-fluids are two of those crucial problems.

Acknowledgments

Jin Qi thanks Yibing Chen for his kind discussion on adaptive mesh method. Yue Wang appreciates Professor Shuanghu Wang for his kind guidance. Our work is supported by NSFC (91130021). Jin Qi is supported by NSFC (1171037, 11201033) and CAEP under project 2012A0202010. Jiequan Li is supported by NSFC (91130021,11371063,11031001), the Doctoral program from Educational Ministry (20130003110004) and an open project from Institute of Applied Physics and Computational Mathematics, Beijing.

References

[1] R. Abgrall, A review of residual distribution schemes for hyperbolic and parabolic problems: the July 2010 state of the art, Commun. Comput. Phys., 11 (2012), 1043–1080.
[2] R. Abgrall and S. Karni, Computations of compressible multifluids, J. Comput. Phys., 169 (2001), 594–623.
[3] D. Benson, Computations methods in Lagrangian and Eulerian hydrocodes, Comput. Methods Appl. Mech. Eng., 99(2-3) (1992), 235–394.
[4] M. Ben-Artzi and J. Falcovitz, A second-order Godunov-type scheme for compressible fluid dynamics, J. Comput. Phys., 55 (1984), 1–32.
[5] M. Ben-Artzi, The generalized Riemann problem for reactive flows, J. Comput. Phys., 81 (1989), 70–101.
[6] M. Ben-Artzi and J. Falcovitz, An upwind second-order scheme for compressible duct flows, SIAM J. Sci. Stat. Comput., 7 (1986), 744–768.
[7] M. Ben-Artzi and J. Falcovitz, Generalized Riemann Problems in Computational Fluid Dynamics, Cambridge University Press, 2003.
[8] M. Ben-Artzi and J. Li, Hyperbolic balance laws: Riemann invariants and the generalized Riemann problem, Numer. Math., 106(3) (2007), 369–425.
[9] M. Ben-Artzi, J. Li and G. Warnecke, A direct Eulerian GRP scheme for compressible fluid flows, J. Comput. Phys., 218 (2006), 19–34.
[10] J. Brackbill and J. Saltzman, Adaptive zoning for singular problems in two-dimensions, J. Comput. Phys., 46 (1982), 342–368.
[11] J. Brackbill, An adaptive grid with directional control, J. Comput. Phys., 108 (1993), 38–50.
[12] W. Cao, W. Huang and R. Russell, A study of monitor functions for two-dimensional adaptive mesh generation, SIAM J. Sci. Comput., 20 (1999), 1978–1999.
[13] A. van Dam and P. Zegeling, Balanced monitoring of flow phenomena in moving mesh methods, Commun. Comput. Phys., 7 (2010), 138–170.
[14] X. Deng, M. Mao, G. Tu, H. Zhang and Y. Zhang, High-order and high accurate CFD methods and their applications for complex grid problems, Commun. Comput. Phys., 11 (2012), 1081–1102.
[15] J. Falcovitz, G. Alfandary and G. Hanoch, A 2-D conservation laws scheme for compressible ows with moving boundaries, J. Comput. Phys., 138 (1997), 83–102.
[16] J. Falcovitz and A. Birman, A singularities tracking conservation laws scheme for compressible duct flows, J. Comput. Phys., 115 (1994), 431–439.
[17] - E. Han, J. Li and H. Tang, An adaptive GRP scheme for compressible fluid flows, J. Comput. Phys., 229 (2010), 1448–1466.

[18] E. Han, J. Li and H. Tang, Accuracy of the adaptive GRP scheme and the simulation of 2-D Riemann problems for compressible Euler equations, Commun. Comput. Phys., 10 (2011), 577–606.
[19] P. He and H. Tang, An adaptive moving mesh method for two-dimensional relativistic hydrodynamics, Commun. Comput. Phys., 11(2012), 114–146.
[20] C. Hirt, A. Amsden and J. Cook, An arbitrary Lagrangian-Eulerian computing method for all flow speeds, J. Comput. Phys., 135 (1997), 203–216.
[21] W. Huang, Variational mesh adaptation: isotropy and equidistribution, J. Comput. Phys., 174(2) (2001), 903–924.
[22] Y. Di, R. Li, T. Tang and P. Zhang, Moving mesh finite element methods for the incompressible Navier-Stokes equations, SIAM J. Sci. Comput., 26 (2005), 1036–1056.
[23] J. Li and G. Chen, The generalized Riemann problem method for the shallow water equations with bottom topography, Int. J. Numer. Methods Eng., 65 (2006), 834–862.
[24] J. Li, T. Liu and Z. Sun, Implementation of the GRP scheme for computing radially symmetric compressible fluid flows, J. Comput. Phys., 228 (2009), 5867–5887.
[25] J. Li and Z. Sun, Remark on the generalized Riemann problem method for compressible fluid flows, J. Comput. Phys., 222(2) (2007), 796–808.
[26] M. Maron and R. Lopez, Numerical Analysis, Wadsworth, 1991.
[27] L. Margolin, Introduction to "an arbitrary Lagrangian-Eulerian computing method for all flow speeds", J. Comput. Phys., 135(2) (1997), 198–202.
[28] G. Ni, S. Jiang and S. Wang, A remapping-free, efficient Riemann-solvers based, ALE method for multi-material fluids with general EOS, Comput. Fluids, 71 (2013), 19–27.
[29] G. Ni, S. Jiang and K. Xu, Remapping-free ALE-type kinetic method for flow computations, J. Comput. Phys., 228 (2009), 3154–3171.
[30] H. Tang and T. Tang, Adaptive mesh methods for one- and two-dimensional hyperbolic conservation laws, SIAM. J. Numer. Anal., 41(2) (2003), 487–515.
[31] T. Tang, Moving mesh methods for computational fluid dynamics, Contemp. Math., 383 (2005), 185–218.
[32] Z. Teng, Modified equation for adaptive monotone difference schemes and its convergent analysis, Math. Comput., 77 (2008), 1453–1465.
[33] B. Tian, W. Shen, S. Jiang, S. Wang and Y. Liu, An arbitrary Lagrangian-Eulerian method based on the adaptive Riemann solvers for general equations of state, Int. J. Numer. Mech. Fluids, 59 (2009), 1217–1240.
[34] B. Tian, W. Shen, S. Jiang, S. Wang and Y. Liu, A Global arbitrary Lagrangian-Eulerian method for stratified Richtmyer-Meshkov instability, Comput. Fluids, 46(1) (2011), 113–121.
[35] E. Toro, Riemann Solvers and Numerical Methods for Fluid Dynamics, Springer, 2009.
[36] C. Wang, H. Tang and T. Liu, An adaptive ghost fluid finite volume method for compressible gasCwater simulations, J. Comput. Phys., 227 (2008), 6385–6409.
[37] A. Winslow, Numerical solution of the quasi-linear Poisson equation, J. Comput. Phys., 1 (1967), 149–172.